DESIGN AND EXPERIMENTAL EVALUATION OF A CIRCULAR FURROWER FOR CITRUS ORCHARDS

/

柑橘果园绕树环形开沟机的设计与试验

Mingzhen LI[1,2], Jiaqi FENG[1,2], Xiaodong YI[1,2], Liang MENG[1,2], Shanjun LI[1,2], Haibing PAN*[1,2],

[1)] Huazhong Agricultural University, Wuhan 430070, China;

[2)] Key Laboratory of Agricultural Equipment for the Middle and Lower Reaches of the Yangtze River, Ministry of Agriculture and Rural Affairs; Wuhan 430070, China.

Corresponding author: Mingzhen LI

Tel: +86 15527955411; E-mail: mingzhen_li@mail.Hzau.Edu.cn

Tel: +86 15907127680; E-mail: phb@mail.hzau.edu.cn

DOI: https://doi.org/10.35633/inmateh-78-87

Keywords: *ditching machine, circular ditch, citrus tree*

ABSTRACT

In response to the difficulties and unsatisfactory performance of existing trenching machines in forming circular trenches for fertilization in citrus orchards, a novel ring-shaped trenching machine designed for around-tree operation was developed. The overall structure and working principle of the machine are presented, and the key components—including the drive system, trenching unit, lifting mechanism of the trenching head, and transmission reducer—were designed and theoretically analyzed. Stability analysis of the machine shows that the limiting overturning angle and slip angle are 53.9° and 34.8°, respectively, indicating that the machine meets the operational requirements of citrus orchard conditions. Considering the soil characteristics of citrus orchards, the optimal working parameters were determined through EDEM simulation: a trench depth of 250 mm, cutter head rotational speed of 190 r/min, and travel speed of 0.565 km/h. Field performance tests conducted on a prototype showed that the average radius of the circular trench was 138 cm, and the trench depth stability coefficient reached 91.8%. The operational performance of the machine meets the agronomic requirements for circular trench fertilization in citrus orchards and complies with the relevant standards for orchard trenching and fertilization equipment.

摘要

针对柑橘果园环沟施肥作业中，现有开沟机存在开环形沟困难、开环形沟效果不理想等问题，设计了一款柑橘果园绕树环形开沟机。阐述了整机结构与工作原理，开展了驱动装置、开沟装置、开沟头升降装置、牙嵌式离合机构、传动减速器各关键部件的设计与理论分析。对整机稳定性进行分析，其极限倾翻角、滑移角分别为 53.9°和 34.8°，整机满足柑橘果园作业环境；结合柑橘果园土壤环境，通过 EDEM 软件仿真，确定了最优工作参数：开沟深度 250 mm，刀头转速 190 r/min，行进速度 0.565 km/h，样机试制后田间性能试验显示，开环形沟半径均值为 138 cm，开环形沟深度稳定性系数为 91.8%。整机作业质量满足柑橘果园开环沟施肥农艺要求，满足果园开沟施肥机作业质量标准。

INTRODUCTION

China has a large proportion of widely distributed hilly and mountainous terrain (*Zheng et al., 2020*). These areas exhibit significant altitude variations, excellent light and heat conditions, and large diurnal temperature differences, which are highly conducive to nutrient accumulation in fruits (*Wang et al., 2016*). Consequently, hilly and mountainous regions have become major production areas for fruits. The fibrous roots of citrus trees are predominantly concentrated within 0–400 mm depth below the canopy drip line (*Ning, 2021; Wang et al., 2023*). Therefore, excavating a circular fertilization trench along the canopy drip line can effectively reduce the migration distance of fertilizers to the root system, facilitating nutrient release and root absorption. This approach enables efficient fertilizer use with reduced application rates, precise fertilization, and uniform nutrient distribution, a method known as circular trench fertilization. However, due to the complexity of the trenching process, the development of corresponding circular trenching machines is challenging. Currently, most trenching machines are designed for straight-line trenching, struggling with poor performance in forming circular trenches. Research on equipment specifically for circular trenching remains limited (*Wei et al., 2020*), failing to meet the growing demands of the fruit industry (*Wang et al., 2021*).

Domestic research on trenching machines started relatively late but has achieved significant results. *Qin Kuan et al.* developed a reciprocating trenching and loosening machine (*Qin et al., 2024*). By analyzing manual shovel-soil models, they improved the trench depth stability coefficient (*Qin et al., 2021*). *Chen Yufeng* designed a chain-type trenching machine for camellia forests, which operates stably and creates neat trenches meeting agronomic requirements (*Chen et al., 2023*). Foreign research, with an earlier start, features mature technology. The large trenching machine developed by Canada's BRON Company boasts a simple structure and high reliability (*Correa J. et al., 2019; Mudarisov S. et al., 2022*). The Trencor T17 trenching machine from the US-based Trencor Company offers adjustable depth, can remove loose soil from and compact the trench bottom, and possesses remote monitoring capabilities (*Yang et al., 2023; Zhang et al., 2020*). While these machines provide valuable references, they still face difficulties in forming small-radius circular trenches and often yield unsatisfactory results in such operations within hilly and mountainous citrus orchards.

In the context of citrus orchards in hilly and mountainous areas (*Liu et al., 2019; Song et al., 2019; Wang et al., 2019*), this study addresses the problems of difficulty in forming small-radius trenches and suboptimal trenching performance associated with traditional trenching machines during operation (*Wangi et al., 2018*). A small-radius circular trenching machine for citrus trees in these terrains was developed (*Song et al., 2019*) and subjected to relevant tests. It is hoped that this machine can provide a reference for research related to circular trenching equipment for citrus orchards (*Zhang et al., 2021*).

MATERIALS AND METHODS

1. Structure Design and Working Principle

1.1 Holistic Structure Design

The small-radius circular trenching machine for citrus trees (*Zhu et al., 2023*) primarily consists of a trenching unit, a drive system, a lifting mechanism for the trenching cutter head, a jaw clutch mechanism, a transmission reducer, and a machine frame. The overall structure of the machine is illustrated in Figure 1, and its main technical parameters are listed in Table 1.

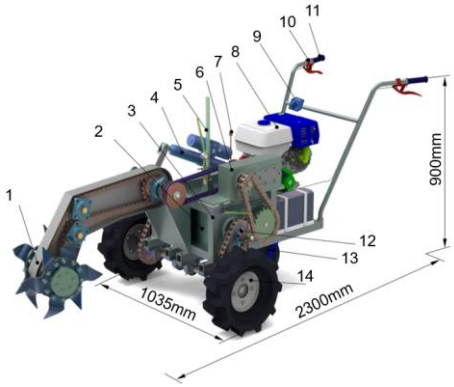

Fig. 1 - Structural Representation of a Self-Driving Orchard Circular Trenching Machine

1. Trenching unit; 2. Transmission case; 3. Frame; 4. Lifting mechanism of the trenching cutter head; 5. Gearshift mechanism; 6. Transmission reducer; 7. Clutch pulley of the trenching cutter head; 8. Engine; 9. Changeover switch; 10. Self-locking clutch grip handle; 11. Handlebar; 12. Jaw clutch mechanism; 13. Caster wheel; 14. Drive wheel

Table 1

Integrated Machine Performance Metrics

Performance indicators	Value
Total machine mass	84 kg
Engine power	5.5 kw
Trench depth	250 mm
Trench radius	136 cm
Circular trenching travel speed	0.2 m/s
Reverse travel speed	0.7 m/s

1.2 Working Principle

The trenching machine features three gear positions: circular trenching gear, linear trenching gear, and reverse travel gear. Its overall transmission principle is illustrated in Figure 2. During circular trenching operation, the engine is started. The self-locking clutch grip handle is squeezed and locked to disconnect the transmission from the drive wheels.

Then, the gearshift mechanism is engaged to select the circular trenching gear on the drive transmission case. The clutch pulley closes, driving the trenching cutter head into rotation. Subsequently, the changeover switch is toggled to lower the cutter head into the soil. Once the desired position is reached, the clutch grip handle is released, and the machine proceeds with self-propelled trenching. Upon completion, the engine is shut off, and the changeover switch is moved in the opposite direction to raise the trenching cutter head to a safe height, thereby concluding the entire circular trenching operation.

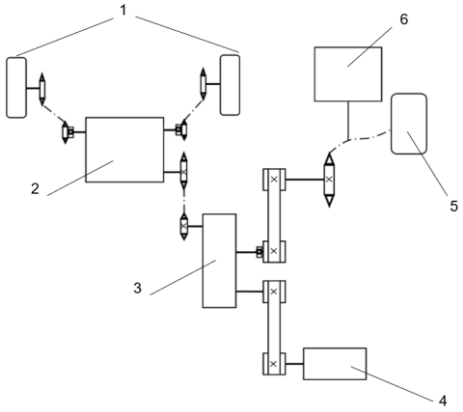

Fig. 2 - General transmission principle diagram of the whole machine

1. Drive wheel; 2. Transmission case; 3. Transmission reducer; 4. Engine; 5. Trenching cutter head; 6. Trenching cutter head lifting mechanism

2. Design and Analysis of Key Components

2.1 Design and Analysis of the Drive System

2.1.1 Kinematic Analysis of the Whole Machine During Trenching

The canopy drip line of fruit trees can be approximately regarded as a circle centered on the tree trunk with a radius of R. This circle also represents the horizontal travel trajectory of the trenching cutter head during the circular trenching operation. The machine adopts a scheme in which the drive transmission case controls the differential speed of the two drive wheels, assisted by a caster wheel for support, to drive the trenching cutter head in forming a circular trench. The circular trenching process can be viewed as the two drive wheels driving the trenching cutter head to perform circular motion around the tree trunk, with the circle's radius being the distance between the cutter head and the trunk, i.e., the circular trench radius R. Selecting any moment during the circular trenching operation, a kinematic model is established as shown in Figure 3.

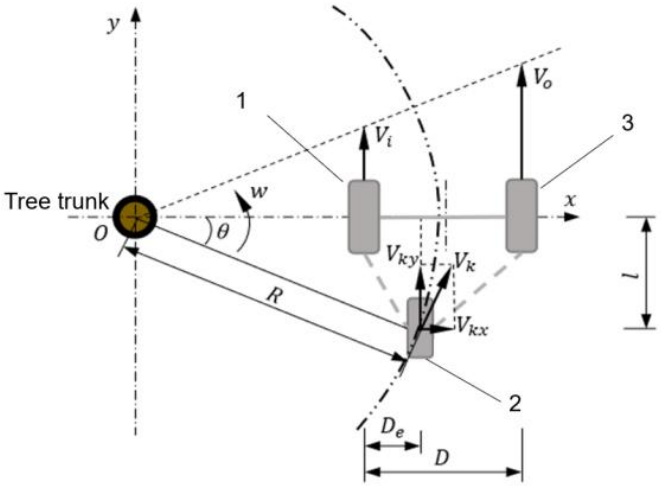

Fig. 3 - Simplified Diagram of the Machine's Circular Trenching Motion

1. Inner wheel; 2. Trenching cutter head; 3. Outer wheel

During the circular trenching operation, the inner and outer wheels drive the whole machine forward, and the trenching cutter head follows accordingly. Simultaneously, the trenching cutter head rotates on its own axis, cutting and ejecting soil, while the spatial relationship among the cutter head, the inner wheel, and the outer wheel remains unchanged. The inner wheel, outer wheel, and trenching cutter head revolve around the tree trunk at the same angular velocity ω (revolution). The linear velocities of the inner and outer wheels are respectively:

$$\begin{cases} V_i = \omega(R\cos\theta - D_e) \\ V_o = \omega(R\cos\theta + D - D_e) \\ \cos\theta = \frac{\sqrt{R^2 - l^2}}{R} \end{cases} \quad (1)$$

where:

V_i -Instantaneous linear velocity of the inner wheel, [m/s];

V_o – Instantaneous linear velocity of the outer wheel, [m/s];

ω – Angular velocity of the whole machine's motion, [rad/s];

θ – Geometric angle between the trenching cutter head, the tree trunk, and the axis of the inner and outer wheels, [°];

l – Wheelbase between the trenching cutter head and the axis of the inner/outer wheels, [m];

D_e – Distance between the trenching cutter head and the central plane of the inner wheel, taken as 0.4 m;

D – Center distance between the inner and outer wheels, taken as 1 m based on the width range of circular fertilization trenches;

R – Radius of the circular trench, tentatively taken as 1.3 m based on the radius range of circular trenches in hilly and mountainous orchards;

During the circular trenching motion, the inner and outer wheels simultaneously undergo rotation. Their linear velocities are:

$$\begin{cases} V_i = \frac{\pi n_i r}{30} \\ V_o = \frac{\pi n_o r}{30} \end{cases} \quad (2)$$

where:

n_i – Rotational speed of the inner wheel, [r/min];

n_o – Rotational speed of the outer heel, [r/min];

r – Radius of the inner/outer wheels, r=0.2 m

From Equations (1) and (2), the speed ratio I_{io} between the inner and outer wheels can be obtained as:

$$I_{io} = \frac{n_i}{n_o} = \frac{\sqrt{R^2 - l^2} - D_e}{\sqrt{R^2 - l^2} + D - D_e} \quad (3)$$

As can be seen from equation (3), the speed ratio between the inner and outer drive wheels is independent of the travel speed of the machine, and there exists a definite functional relationship between the circular trench radius and the speed ratio of the inner and outer drive wheels. Therefore, given that other parameters remain constant and the speed ratio of the inner and outer drive wheels is fixed, changing only the travel speed will not affect the size of the circular trench radius.

The motion linear velocity V_k of the trenching cutter head has components in the x-direction V_{kx} and in the y-direction V_{ky}, which are respectively expressed as:

$$\begin{cases} V_{kx} = V_k \sin\theta \\ V_{ky} = V_k \cos\theta \\ \cos\theta = \frac{\sqrt{R^2 - l^2}}{R} \end{cases} \quad (4)$$

V_{ky} aligns with the travel direction of the trenching cutter head. A larger V_{ky} is more conducive to the circular motion of the entire machine. Conversely, V_{kx} is perpendicular to the trenching travel direction, and a smaller V_{kx} is more favorable for the machine's circular movement. From Equation (4), it can be deduced that the condition l=0 is optimal for the machine's motion. Therefore, the wheelbase between the trenching cutter head and the axis of the inner and outer wheels is preliminarily set to 0. Combining this with Equation (3), the differential speed ratio between the inner and outer wheels is derived as I_{io}=9/19. This result provides a reference for determining the optimal reduction ratio of the subsequent reducer, thereby ensuring the required radius of the circular trench.

2.1.2 Transmission principle of gear positions in the drive transmission case

The drive gearbox can control the rotational speeds of the inner and outer wheels through gear shifting, enabling the trencher to dig circular trenches, linear trenches, and achieve rapid reverse straight-line movement.

Considering the characteristics of circular trenching operations and agricultural requirements, the initial set linear traveling speeds are V_{k1} = 0.2 m/s for circular trenching, V_{k2} = 0.27 m/s for linear trenching, and V_{k3} = 0.7 m/s for rapid reverse straight-line movement. The gear shifting principle is illustrated in Figure 4.

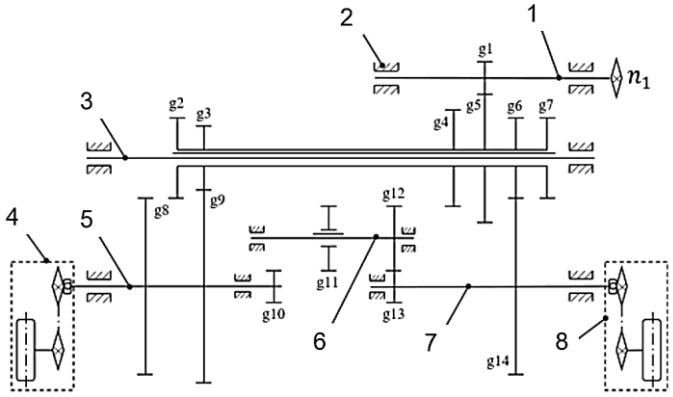

Fig. 4 - Simplified Diagram of the Drive Gearbox Transmission Principle

1. Input shaft; 2. Housing; 3. Gear shift shaft; 4. Inner wheel; 5. Left output shaft; 6. Transmission shaft; 7. Right output shaft; 8. Outer wheel

2.2 Design and analysis of the trenching unit

2.2.1 Selection and design of trenching blades

Taking into comprehensive consideration the soil operating conditions in traditional Chinese orchards and hilly-mountainous orchards (*Shi et al., 2019*), the cup-shaped curved blade (*Kang et al., 2017*), which offers excellent soil cutting, soil throwing, anti-clogging, and strength performance, was selected as the trenching tool. Since a single-disc trenching cutter head has low flexibility and an unbalanced reaction torque, making it unsuitable for hilly and mountainous terrain, a dual-disc trenching cutter head design was adopted.

Currently, there is no definitive standard for selecting the cutting tip's rotary diameter. This section employs an empirical formula (5) to determine the cutting tip's rotary diameter D_k.

$$D_k = (1.2\sim1.4)H \tag{5}$$

where: H –target trench depth, [mm].

The process requirements for orchard fertilization trenches specify a trench depth range of 150–350 mm. According to Formula (5), the corresponding cutting tip rotary diameter D_k ranges from 180 to 490 mm.

The smaller the trenching cutter head, the more conducive it is to the smooth progress of the entire machine during circular trenching operations. On the premise of meeting the depth requirement, the cutting tip rotary diameter is selected as D_k= 400 mm.

To ensure that the soil cutting volume of each trenching blade is similar, and to achieve a neat trench wall and bottom surface after operation, the blades are arranged uniformly. Additionally, the axial angle between adjacent blades is maximized as much as possible to prevent clogging caused by soil accumulation or stones. Based on the above considerations, taking the blade arrangement on one side of cutter disc Ⅰ as an example: within the axial projection circle of the blade holder, three left-handed trenching blades and three right-handed trenching blades are installed evenly. The three left-handed blades are mounted on one side of the holder at 120° intervals, while the three right-handed blades are mounted on the opposite side also at 120° intervals. All left-handed blades and right-handed blades are staggered by a phase angle of 60°.

The rotational speed range of the cutter head is determined by the linear speed range of rotary tiller blades, v =(3.5~6.0) m/s, in conjunction with Equation (6).

$$n_k = \frac{60v}{\pi D_k} \tag{6}$$

Based on field measurements of traditional trenching machines in hilly and mountainous orchards, the spacing between trenching blades on the two cutter discs ranges from 50 to 60 mm. To minimize the distance between the two cutter discs and reduce the size of the soil ridge formed on the bottom of the trench, the two cutter discs are arranged in an inclined configuration. Under the condition of ensuring no interference between the trenching blades and the transmission case, the inclination angle is increased to reduce the disc spacing. Ultimately, the inclination angle of the cutter discs is determined as α = 14°, with a center-to-center distance of 45 mm between the two discs. The installation and arrangement scheme of the cutter discs and blades is shown in Figure 5.

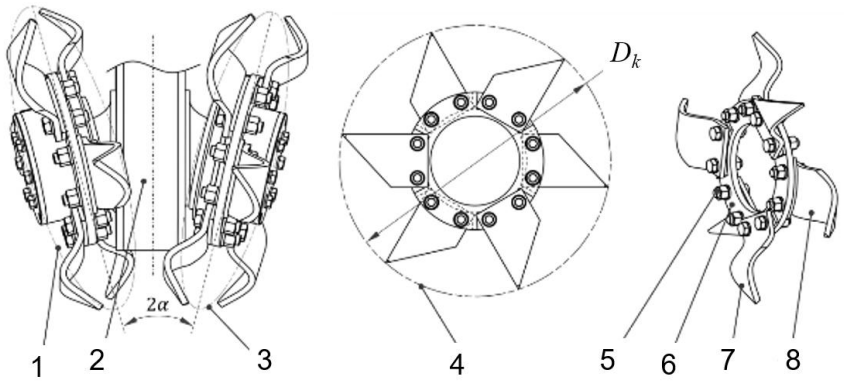

Fig. 5 - Arrangement Scheme for the Installation of Ditching Blades

1. Cutter disc Ⅰ; 2. Transmission case; 3. Cutter disc Ⅱ; 4. Cutting tip trajectory; 5. Fastening bolt; 6. Blade holder; 7. Left-hand trenching blade; 8. Right-hand trenching blade

2.2.2 Dynamic and power analysis of trenching

Dynamic analysis is performed on a trencher conducting trenching operations in an uphill state. The force analysis is illustrated in Figure 6a and Figure 6b. During circular trenching, the machine moves along a curved path, and the total resistance F is:

$$F = F_t + F_g + F_r + F_c \tag{7}$$

where:

F_t -- Steering resistance during circular trenching, [N];

F_g--Gravitational component when moving uphill, [N];

F_r--Rolling resistance during travel, [N];

F_c--Soil cutting resistance, [N]

where:

$$\begin{cases} F_t = \mu_t (G\cos\theta + F_c/2) L/2R \\ F_g = G\sin\theta \\ F_r = \mu G\cos\theta \\ Fc = KBH \end{cases} \tag{8}$$

where:

μ_t--Steering resistance coefficient, taken as 0.6;

G--Total machine weight [N];

L--Wheel track of the drive wheels, [m];

R--Radius of the circular trench, [m];

θ--Maximum slope angle of hilly and mountainous terrain, θ =25 ;

μ--Rolling resistance coefficient, taken as 0.2;

K--Specific resistance of citrus orchards in hilly and mountainous areas, K=120 kPa/m^2;

B--Width of the circular trench, [m];

H--Depth of the circular trench, [m].

The required engine power P can be expressed as:

$$\begin{cases} P_t = Fv \\ P = \frac{P_t}{\eta} \end{cases} \tag{9}$$

where: P_t --Tractive power, [W];

P--Required engine power, [W];

v--Travel speed for circular trenching, [m/s];

η--Efficiency of the transmission system, taken as 0.65.

Based on the empirical data on transmission efficiency provided in the Mechanical Design Handbook, and taking into account the gear drives, chain drives, and bearing arrangements adopted in this machine, the overall transmission efficiency from the engine output shaft to the driving wheels was estimated.

After considering additional power losses caused by harsh field operating conditions (such as dust and mud intrusion, inadequate lubrication, and assembly errors), a conservative overall efficiency of η = 0.65 was adopted for the calculations.

Calculation yields a required engine power of 5.12 kW. Therefore, a 5.5 kW gasoline engine was selected.

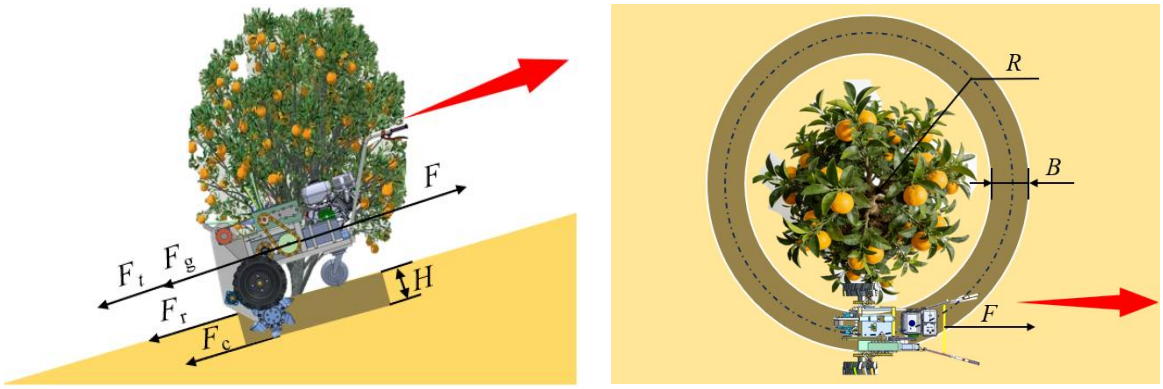

(a) (b)

Fig. 6 - Dynamic analysis of uphill circular trenching

2.3 Design and analysis of the trenching cutter head lifting mechanism

The schematic diagram of the kinematic principle of the folding lifting mechanism for the trenching cutter head is shown in Figure 8. The lifting device is actuated by an electro-hydraulic system that extends the push rod outward. According to the geometric relationships illustrated in Figure 7, points C and C' represent the stroke limit positions of the electro-hydraulic push rod. Based on the Law of Cosines, the following relationship can be derived:

$$\begin{cases} l_{AC}^2 = l_{AB}^2 + l_{BC}^2 - 2l_{AB}l_{BC}\cos\beta \\ l_{AC'}^2 = l_{AB}^2 + l_{BC}^2 - 2l_{AB}l_{BC'}\cos\beta' \end{cases} \quad (10)$$

where:

$l_{AC}, l_{AB}, l_{BC}, l_{AC'}, l_{BC'}$--Lengths of the linkage segments AC, AB, BC, AC', BC', l_{AB}=530 mm, $l_{BC} = l_{BC'}$=196 mm;

β--The angle between linkage segment AB and linkage segment BC, β = 134°;

β'--The angle between linkage segment AB and linkage segment BC′, β' = 58°.

Based on Equation (10), the calculated lengths are l_{AC}=680.9 mm and $l_{AC'}$=457.4 mm. Thus, the stroke range of the push rod is 457.4 mm≤ L_{AC} ≤680.9 mm. Accordingly, the HB-DJ750 electro-hydraulic push rod was selected. This electro-hydraulic push rod integrates a 12 V DC motor drive system, with a standard stroke of 300 mm, a minimum installation distance of 450 mm, a rated dynamic load of 8000 N, and a rated static load of 15000 N. It provides both pushing and pulling capabilities and is suitable for the highly bumpy and shock-prone environments typical of hilly and mountainous orchards.

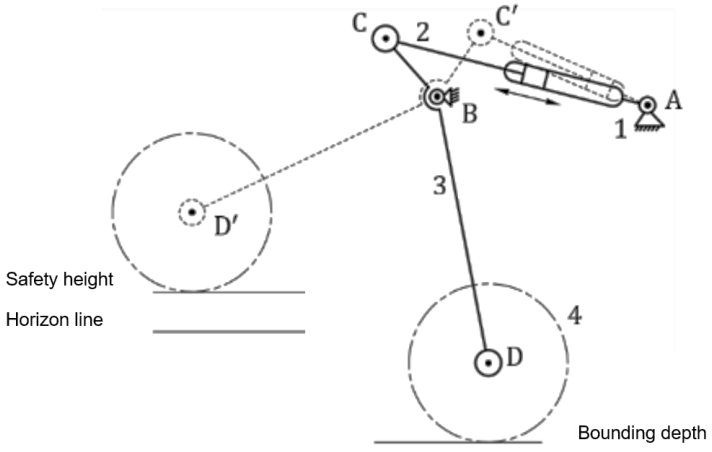

Fig. 7 - Simplified Diagram of the Folding and Lifting Mechanism Motion for the Ditching Cutter Head

2.4 Operating principle of the transmission reducer

To accommodate the different speed requirements for trenching and traveling, the trencher utilizes a single engine to drive both the transmission case and the trenching unit, enabling automatic propulsion and trenching (*Peng et al., 2018; Zhang et al., 2024*). The structural principle of the transmission reducer is illustrated in Figure 8.

The rotational speed output by the engine is transmitted via the input pulley to the input shaft. After undergoing two-stage speed reduction, the power is transferred to output shaft Ⅰ. Following three-stage reduction, the power is further transmitted to output shaft Ⅱ. Output shaft Ⅰ drives the trenching unit through the trenching clutch pulley, while output shaft Ⅱ drives the transmission case via the transmission chain wheel.

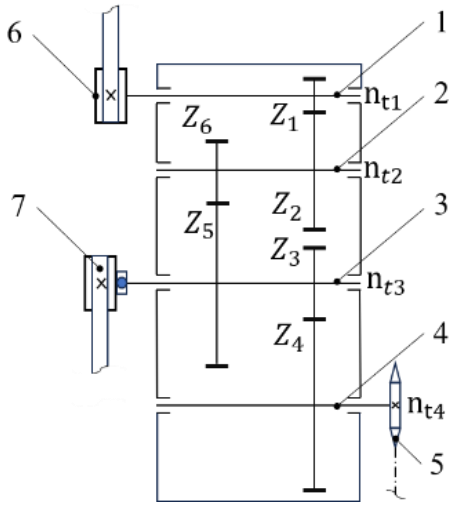

Fig. 8 - Schematic of the Transmission Reducer Structure

1. Input shaft; 2. Drive shaft; 3. Output shaft Ⅰ; 4. Output shaft Ⅱ; 5. Transmission case sprocket; 6. Input pulley; 7. Trenching clutch pulley

3. Operational Stability of the Whole Machine

The operational stability of the trencher primarily considers its lateral and longitudinal stability when working in hilly and mountainous citrus orchards. By introducing the limit overturning angle and the limit slip angle as key evaluation indicators, a systematic assessment of the machine's lateral and longitudinal stability has been conducted. A multi-dimensional stability evaluation model (*Liu et al., 2024*) was constructed to provide a theoretical basis for optimizing the safe operational parameters of the trencher. Based on the mass-property module of SolidWorks software, the position of the whole machine's center of mass was measured. The structural parameters involved in the analysis of the whole machine's operational stability are listed in Table 2.

Table 2

Structural parameters related to the stability analysis of the entire machine's operation

Parameters	Value/mm
Distance between the axes of the drive wheel and the caster wheel	545
Horizontal distance between the drive wheel and the center of mass	270
Offset of the center of mass	5
Vertical distance from the center of mass to the ground	395
Width of the drive wheel	145
Spacing between the two drive wheels	929

3.1 Lateral stability

Schematic diagram of lateral stability analysis of the small-radius is shown in Figure 9.

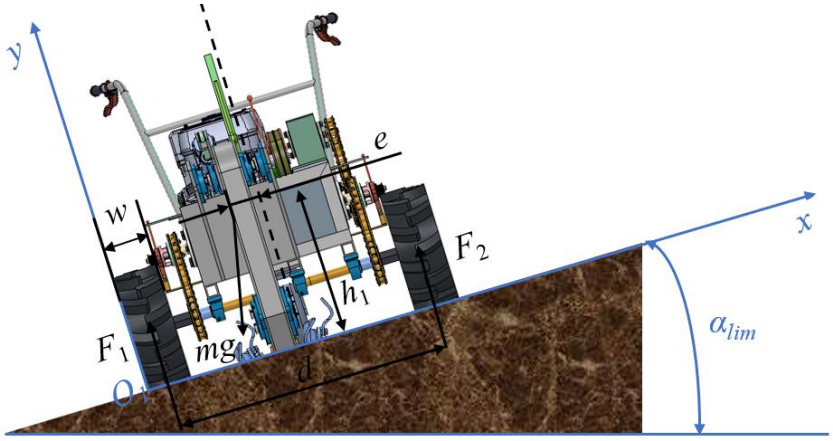

Fig. 9 - Schematic diagram of lateral stability analysis

Taking the positive direction of the x-axis as the reference direction and selecting point O_1 as the moment center, the equilibrium equations for the force system in the xy-plane are established as follows:

$$\begin{cases} F_1 + F_2 - \cos\alpha_{\lim} = 0 \\ F_2 w_z + mg\sin\alpha_{\lim} h = mg\cos\alpha_{\lim}(w_z - e) \\ w_z = d + \dfrac{w}{2} \end{cases} \tag{11}$$

where:

F_1, F_2 - Normal supporting forces exerted by the ground on the left and right wheels, [N];

h_1 - vertical distance from the center of mass to the ground, [mm];

d -spacing between the left and right wheels, [mm];

w - Tread width of driving wheels, [mm];

m--Total mass of the machine, [kg];

e--Lateral offset distance of the center of mass from the longitudinal central plane, [mm];

α_{lim}--Limit overturning angle, [°].

It can be seen from Equation (11) that F_2 is:

$$F_2 = \frac{mg(\dfrac{d+w}{2} + e)\cos\alpha_{\lim} - mg\sin\alpha_{\lim} h}{d + \dfrac{1}{2}w} \tag{12}$$

The condition for the trencher to avoid overturning is that F_2 is greater than or equal to 0. It can be inferred from Equation (11) that:

$$\alpha_{\lim} \le \arctan\frac{d + w + 2e}{2h} \tag{13}$$

Combining Equation (13) and the relevant parameters in Table 2, the value of $\alpha_{\lim}$ is determined to be 53.9°. Considering the topographic characteristics of orchards in China's hilly and mountainous regions, where slopes are predominantly between 5° and 25°, the calculation results indicate that the machine exhibits excellent lateral stability and is well-suited for operation in orchards located in China's hilly and mountainous areas.

3.2 Longitudinal Stability

To simplify the analysis, the trencher during operation is considered stationary relative to the slope, maintaining a state of static equilibrium. On longitudinal slopes, the condition for overall machine stability is that the limit slip angle must be greater than the slope gradients typically found in hilly and mountainous orchards, as illustrated in Figure 12.

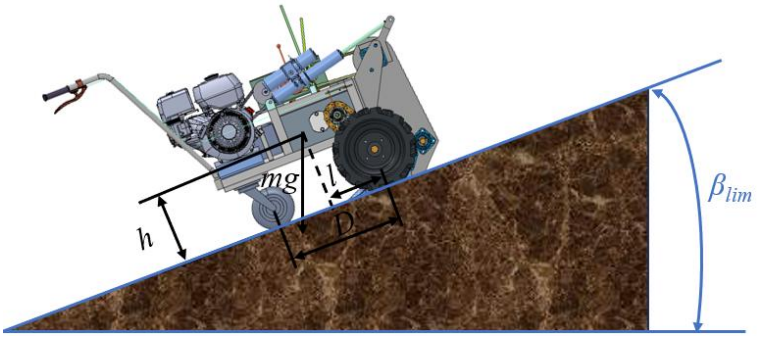

Fig. 10 - Schematic diagram of longitudinal stability analysis

The calculated limit slip angle on longitudinal slopes is

$$\beta_{lim} = \arctan\frac{D-l}{h} \tag{14}$$

where:

D--Distance between the driving wheel and the caster wheel, [mm];

l--Distance between the driving wheel and the center of mass, [mm].

Based on Equation (14), the limit slip angle $\beta_{\lim}$ for the small-radius circular trencher used in hilly-mountainous citrus orchards is calculated as 34.8°, which is above 25° and therefore meets the operational requirements of citrus orchards in such terrain.

4 Discrete Element Method

4.1 Establishment of Simulation Parameters and Models

4.1.1 Determination of Simulation Parameters

In a 2017 study by Wu Tao et al. (*Wu et al., 2017*), the "Hertz-Mindlin with JKR (Johnson–Kendall–Roberts theory)" contact model was adopted to simulate the influence of cohesive forces between viscous soil particles on particle motion. Through simulation calibration via the EDEM (*Zhu et al., 2020; Zdancevičius E et al., 2017*), a regression model was established between the angle of repose and the JKR surface energy, the coefficient of restitution between particles, the static friction coefficient, and the rolling friction coefficient. Utilizing the optimization function of Design-Expert software, the optimal parameter combination targeting an angle of repose of 60.4° was determined as follows: JKR surface energy 15.3 J·m⁻², inter-particle restitution coefficient 0.74, static friction coefficient 0.66, and rolling friction coefficient 0.26. These parameters were used to generate a small particle bed measuring 750 mm × 750 mm × 400 mm for conducting simulation tests of circular trenching (*Mudarisov S et al., 2022*). The key parameters of the simulation model are listed in Table 3.

Table 3

Key Parameters of the EDEM Simulation Model

Item	Parameter	Value
Soil Particles	Poisson's Ratio	0.40
	Shear Modulus [Pa]	2.0×107
	Density [kg/m³]	2200
	Particle Radius [mm]	5
	Angle of Repose [°]	60.4
	JKR Surface Energy [J/m²]	15.3
65Mn Trencher Blade	Poisson's Ratio	0.29
	Shear Modulus [Pa]	8.19×1010
	Density [kg/m³]	7820
Interaction	Particle-Particle Restitution Coefficient	0.74
	Particle-Particle Static Friction Coefficient	0.66
	Particle-Particle Rolling Friction Coefficient	0.26
	Particle-Blade Restitution Coefficient	0.20
	Particle-Blade Static Friction Coefficient	0.30
	Particle-Blade Rolling Friction Coefficient	0.25

4.2 Test Methods and Experimental Results

4.2.1 Test Methods

Along the stable segment of the circular trenching operation, measurement zones were set at 30° intervals around the central axis of the annular particle bed, resulting in a total of 10 measurement zones, each with a thickness of 20 mm. Using the Manual Selection function, several particles were selected from the trench bottom within each zone, and the Z-axis coordinate values of the selected particles were exported. The average Z-coordinate of these particles was then calculated, defined as the distance a_i from the particles at the trench bottom to the base of the particle bed. The trench depth value h_i for each measurement zone, the average trench depth h, and the depth stability coefficient U_h can be calculated using the following expressions:

$$\begin{cases} h_i = H_0 - a_i \\ h = \dfrac{\sum_1^N h_i}{N} \\ U_h = \left(1 - \sqrt{\dfrac{\sum_1^N (h_i - h)^2}{h^2(N-1)}}\right) \times 100\% \end{cases} \tag{15}$$

where:

N--Number of measurement zones，N=10;

H_0--Total height of the particle bed，H_0=400 [mm].

The circular trench depth compliance coefficient Q_h is defined as another metric for evaluating trenching quality from the dimensional perspective of depth, ensuring the trench depth meets the required standards. The defining expression for Q_h is given in Equation (16).

$$Q_h = \frac{h}{h_0} \times 100\% \tag{16}$$

where:

h_0--Target trench depth, [mm]

h --Actual average trench depth in the simulation model, [mm]

4.2.2 Test Results

The design scheme and results of the central composite design (CCD) simulation experiment are shown in Table 4, where X_1, X_2, and X_3 represent the coded values of the factors. The results of each experimental design and evaluation index are shown in Table 4, Table 5 and Table 6.

Table 4

Schemes and Outcomes of Simulation Experiments

Number	Experimental Factors			Average trench depth h / mm	Depth stability coefficient U_h / %	Depth compliance coefficient Q_h / %
	X_1	X_2	X_3			
1	-1	-1	-1	158.37	78.32	83.35
2	1	-1	-1	142.27	79.23	74.88
3	-1	1	-1	233.99	81.04	75.48
4	1	1	-1	221.74	88.02	71.53
5	-1	-1	1	143.53	76.02	75.54
6	1	-1	1	134.67	80.16	70.88
7	-1	1	1	179.55	72.11	57.92
8	1	1	1	189.69	83.54	61.19
9	-1.682	0	0	189.68	77.09	75.87
10	1.682	0	0	177.80	85.18	71.12
11	0	-1.682	0	118.92	75.89	79.28
12	0	1.682	0	217.67	80.32	62.19
13	0	0	-1.682	218.90	91.16	87.56
14	0	0	1.682	155.90	80.23	62.36
15	0	0	0	205.55	88.09	82.22

Number	Experimental Factors			Average trench depth h / mm	Depth stability coefficient U_h / %	Depth compliance coefficient Q_h / %
	X_1	X_2	X_3			
16	0	0	0	203.83	89.19	81.53
17	0	0	0	202.93	85.07	81.17
18	0	0	0	208.68	86.28	83.47
19	0	0	0	201.93	87.45	80.77
20	0	0	0	198.30	90.16	79.32

Table 5

Variance Analysis of Simulation Experiment Regression Model 1

Source	Sum of Squares	df	Mean Square	P-Value
Model 1	529.38	9	58.82	$<0.0001^{**}$
X_1	100.60	1	100.60	0.0002^{**}
X_2	24.87	1	24.87	0.0191^{*}
X_3	80.52	1	80.52	0.0005^{**}
X_1X_2	22.31	1	22.31	0.0247^{*}
X_1X_3	7.37	1	7.37	0.1598
X_2X_3	18.12	1	18.12	0.0386^{*}
X_1^2	99.99	1	99.99	0.0002^{**}
X_2^2	197.87	1	197.87	$<0.0001^{**}$
X_3^2	15.05	1	15.05	0.0552
Lack of Fit	14.55	5	2.91	0.5758

Note: ** indicates the item is highly significant (P < 0.01); * indicates the item is significant (P < 0.05). Items with a P-value greater than 0.05 are considered non-significant.

Table 6

Variance Analysis of Simulation Experiment Regression Model 2

Source	Sum of Squares	df	Mean Square	P-Value
Model 2	1316.10	9	146.23	$<0.0001^{**}$
X_1	34.79	1	34.79	0.0124^{*}
X_2	331.37	1	331.37	$<0.0001^{**}$
X_3	493.45	1	493.45	$<0.0001^{**}$
X_1X_2	19.38	1	19.38	0.0466^{*}
X_1X_3	15.21	1	15.21	0.0721
X_2X_3	32.36	1	32.36	0.0150^{*}
X_1^2	134.50	1	134.50	0.0001^{**}
X_2^2	234.15	1	234.15	$<0.0001^{**}$
X_3^2	92.76	1	92.76	0.0006^{*}
Lack of Fit	27.87	5	5.57	0.5758
Predicted R2	0.8317			
Adeq Precision	20.2278			

Note: ** indicates that the item is highly significant (P < 0.01); * indicates that the item is significant (P < 0.05). A P-value greater than 0.05 indicates that the item is not significant.

4.2.3 Analysis of Results

Analysis indicates that during the circular trenching process, the blade rotational speed X_1, trenching depth X_2, and traveling speed X_3 have significant effects on the depth stability coefficient U_h and the depth compliance coefficient Q_h of the circular trench. After eliminating the non-significant terms, the second-order regression models relating U_h and Q_h to the significant factors are obtained as shown in Equation (17).

$$\begin{cases} U_h = 87.75 + 2.71X_1 + 1.35X_2 - 2.43X_3 + 1.67X_1X_2 - 1.51X_2X_3 - 2.63X_1^2 - 3.71X_2^2 \\ Q_h = 81.45 - 1.6X_1 - 4.93X_2 - 6.01X_3 + 1.56X_1X_2 - 2.01X_2X_3 - 3.06X_1^2 - 4.03X_2^2 - 2.54X_3^2 \end{cases} \quad (17)$$

The study utilized Design-Expert 13 software to analyze the effects of trenching depth, rotational speed of the blade, and traveling speed on the depth stability coefficient U_h and the depth compliance coefficient Q_h, and generated the response surface plots shown in Figure 11. As can be seen from Figure 11, the order of influence of each factor on both parameters is: trenching depth > rotational speed > traveling speed.

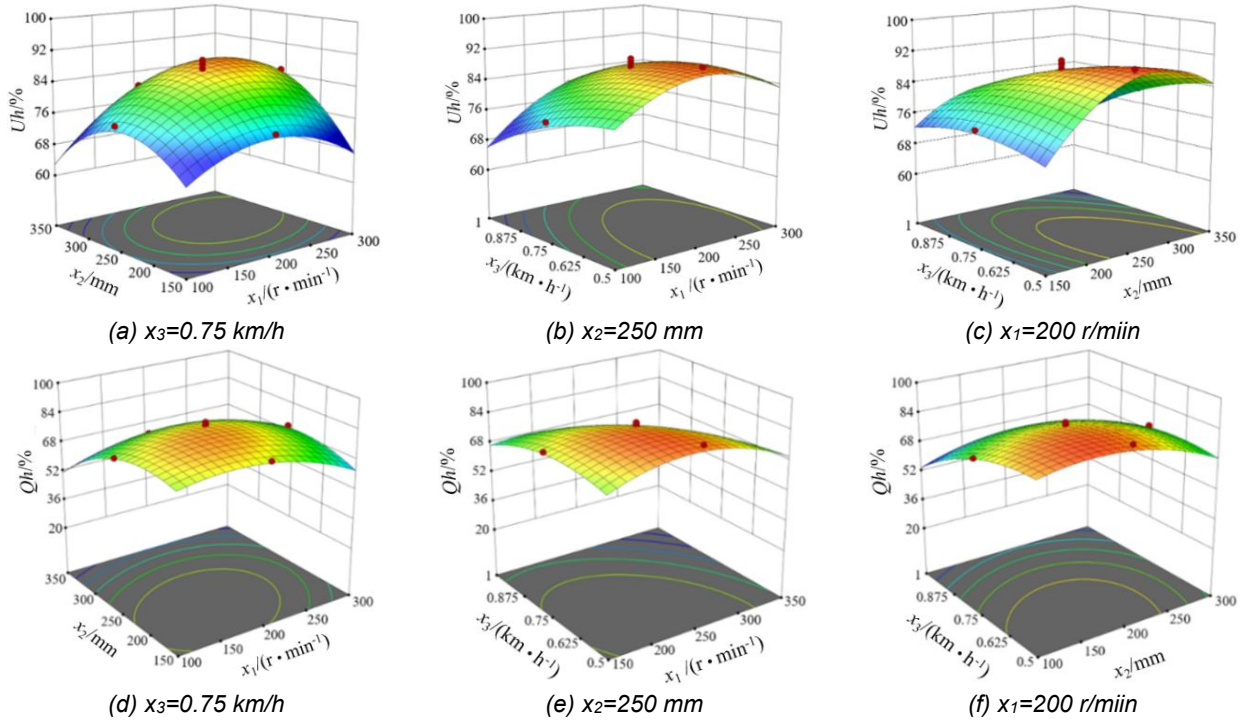

(a) x_3=0.75 km/h (b) x_2=250 mm (c) x_1=200 r/miin

(d) x_3=0.75 km/h (e) x_2=250 mm (f) x_1=200 r/miin

Fig. 11 - The influence of various factors on the stability coefficient and the depth compliance coefficient of the annular groove

(a) and (d) illustrate the effects of trenching depth (x_2) and disc rotation speed (x_1) on the depth stability coefficient (U_h) and depth qualification coefficient (Q_h) when the travel speed (x_3) = 0.75 km/h; (b) and (e) illustrate the effects of travel speed (x_3) and disc rotation speed (x_1) on the depth stability coefficient (U_h) and depth qualification coefficient (Q_h) when the trenching depth (x_2) is 250 mm; (c) and (f) illustrate the effects of travel speed (x_3) and trenching depth (x_2) on the depth stability coefficient (U_h) and depth qualification coefficient (Q_h) when the disc rotation speed (x_1) is 200 r/min.

Based on the aforementioned analysis, a multi-objective optimization was conducted using Design-Expert 13 software, aiming to maximize both the depth stability coefficient and the depth compliance coefficient. The optimal parameters obtained are as follows: trenching depth of 250.91 mm, rotational speed of 190.57 r/min, and traveling speed of 0.565 km/h, corresponding to a depth stability coefficient of 88.93% and a depth compliance coefficient of 85.41%. To facilitate parameter adjustment in practice, the finalized operational parameters for the small-radius circular trencher are set as: rotational speed of 190 r/min, trenching depth of 250 mm, and traveling speed of 0.565 km/h. This provides a basis for regulating the working parameters of the prototype and conducting orchard performance tests.

5 Prototype Performance Tests

5.1 Test Conditions

The prototype performance test was conducted in March 2024 at the experimental base of the Orchard Full-process Mechanization Research Institute, Huazhong Agricultural University. Prior to the test, the soil working parameters in the orchard were measured, including soil moisture content, soil bulk density, and soil compactness. Using a five-point sampling method in the test area, five rectangular plots measuring 500 mm × 500 mm were established as measurement zones. The average soil moisture content in the orchard at depths of 0–100 mm, 100–200 mm, 200–300 mm, and 300–400 mm was measured to be 22.20%, 23.12%, 23.84%, and 24.92%, respectively. The average soil bulk density at these depths was 1.076 g/cm³, 1.344 g/cm³, 1.495 g/cm³, and 1.524 g/cm³, respectively.

The soil compactness values were 2.200 MPa, 3.538 MPa, 5.134 MPa, and 5.788 MPa, respectively. The soil moisture content was measured using a GHHB-009-485-1 soil moisture meter (with a humidity accuracy of ±0.3%), the soil bulk density was sampled and tested using a cutting ring, and the soil compactness was measured using a TYD-2 digital soil hardness meter (with an accuracy of ±1%). The test machine was the self-developed circular trencher for around-tree operation in citrus orchards.

5.2 Test Plan

Two complete circular trenches (designed with a radius of 130 cm) were excavated within the test area, representing two separate trenching operation cycles. In the stable trenching section of each operation cycle, measurement zones were established at 30° intervals around the central axis of the circular trench, resulting in a total of 10 zones per trench. Across both operation cycles, a total of 20 measurement zones were sampled, each with a width of 200 mm. The trenching effect is shown in Figure 12.

Fig. 12 - Views of Circular

This test comprehensively references the test methods specified in 《NY/T 740-2003 Field Trenching Machinery Operation Quality Standard》, 《JB/T 11908-2014 Agricultural Disc Trenchers》, 《DB36/T 1785-2023 Technical Code for Mechanized Trenching and Fertilization in Hilly Orchards》, and DB62/T 2770-2017 Orchard Trenching and Fertilizing Machine - Operation Quality》. The following indicators were selected to evaluate trenching quality: loose soil thickness at the trench bottom, trench surface width, trench bottom width, trench depth, and depth stability coefficient. Among these, the loose soil thickness at the trench bottom, trench surface width, trench bottom width, and trench width are measured and calculated according to the aforementioned standards. The fertilization trench excavated by the self-propelled circular orchard trencher has a trapezoidal cross-section. The dimensional parameters are illustrated in Figure 13, where h_r represents the trench depth, S_f represents the loose soil thickness, B_f represents the trench bottom width, and B_r represents the trench surface width.

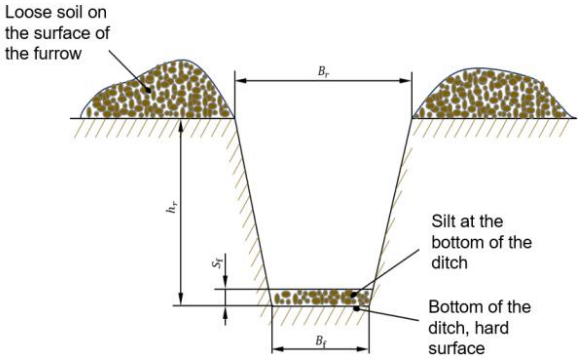

Fig. 13 - Schematic Diagram of Trench Cross-Section

The trench depth and depth stability coefficient are measured and calculated as follows: As shown in Figure 14, within the measurement zone of each operation cycle, after the loose soil thickness at the trench bottom, the trench surface width, and the trench bottom width are determined, a straightedge is placed horizontally across the trench, resting on both sidewalls at the trench surface. Three random measurement points are selected along the trench bottom, and the vertical distance from the straightedge to each of these three points is recorded. The average of these recorded values is taken as the estimated trench depth for that measurement zone. The average trench depth and the depth stability coefficient are then calculated according to Equations (18), (19), and (20).

$$h_r = \frac{\sum_{k=1}^{n} h_{rk}}{n} \tag{18}$$

$$\sigma = \sqrt{\frac{\sum_{k=1}^{n}(h_{rk}-h_r)^2}{n-1}} \tag{19}$$

$$U_r = \left(1 - \frac{\sigma}{h_r}\right) \times 100\% \tag{20}$$

where:

h_r -- Average trench depth, [mm];
h_{rk} --Trench depth in measurement zone k, [mm];
n -- Number of measurement zones, n=20;
σ -- Standard deviation of trench depth;
U_r -- Trench Depth Stability Coefficient.

Fig.14 - Process of Measuring Trench Depth

RESULTS AND DISCUSSION

Based on the aforementioned performance test protocol and measurement methods for each indicator, the measured stability coefficients for the circular trench and the linear trench were 91.8% and 93.2%, respectively. The average radius of the circular trench was 138 cm, which meets the trenching process requirements for citrus orchards in hilly and mountainous areas. The target trench depth for this test was 250 mm, the target trench surface width was 350 mm, and the target trench bottom width was 220 mm. Using the calculation formulas for trenching quality indicators recommended by standards such as 《DB62/T 2770-2017 Orchard Trenching and Fertilizing Machine – Operation Quality》 and 《DB36/T 1785-2023 Technical Code for Mechanized Trenching and Fertilization in Hilly Orchards》, the target indicator values were converted. Combined with the actual test values of the depth stability coefficient, the actual trenching operation quality was evaluated. The assessment results are shown in Table 7.

Table 7

Working Performance of the Ditching Machine

Serial Number	Item Category		Standard Trenching Quality Indicator	Actual Trenching Quality Indicator	
	Item	Type		Circular Trench	Pass/Fail
1	Trenching depth /mm	A	240~260	241.5	Pass
2	Trenching Depth Stability/%		≥80	91.8	Pass
3	Trench Surface Width /mm	B	335~365	357.9	Pass
4	Trench Bottom Width /mm		205~235	233.6	Pass
5	Thickness of Loose Soil at Trench Bottom/mm		≤25	43.2	Fail

As can be seen from Table 7, all Category A indicators meet the standards, while only one item under Category B is qualified. According to the 《DB62/T 2770-2017 Orchard Trenching and Fertilizing Machine—Operation Quality》, the trenching quality of this machine is considered acceptable. The soil in the test orchard used in this prototype trial had higher moisture content and compactness compared to typical cultivated orchard soils, with significantly greater compactness in the deeper soil layers than in the shallower ones.

This dense, deep soil imposed considerable cutting resistance on the trencher blades, leading to difficulties in soil cutting and throwing. Additionally, the surface soil in the test area was relatively fragmented, causing broken soil from both sides of the trench walls to easily slide into the trench bottom due to vibration during operation, resulting in a higher thickness of loose soil at the trench bottom. The orchard selected for this prototype test exhibited relatively high soil moisture content and compactness, which are unfavorable conditions for machinery operation and represent a comparatively harsh orchard soil environment. The fact that the trenching performance remained acceptable under such conditions demonstrates that the prototype is fully capable of operating effectively in orchard environments with soil conditions better than those encountered in this test.

CONCLUSIONS

(1) In response to challenges faced by traditional trenchers when operating in hilly and mountainous orchards—such as difficulty in excavating small-radius circular trenches, suboptimal circular trenching performance, and inadequate adaptability to hilly terrain—this study, considering the technical requirements of circular trench fertilization, proposes an integrated structural design for a small-radius circular trencher specifically tailored for citrus orchard circular trenching.

(2) Analysis of the machine's stability shows that its limit overturning angle and slip angle are 53.9° and 34.8°, respectively, meeting the operational requirements of citrus orchards. Using the depth stability coefficient and depth compliance coefficient as test indicators, and taking trenching depth, blade rotational speed, and travel speed as experimental factors, a central composite simulation test for circular trenching was conducted via EDEM software. With the objective of maximizing both the depth stability coefficient and the depth compliance coefficient, the optimal working parameter combination was determined as follows: trenching depth 250 mm, blade rotational speed 190 r/min, and travel speed 0.565 km/h.

(3) After fabricating and adjusting the prototype according to the design scheme and the optimal parameter combination, the working conditions of the test orchard were first measured, followed by circular and linear trenching trials. The test results indicate that the depth stability coefficient of the circular trench is 91.8%, and the average circular trench radius is 138 cm. In accordance with the standard 《DB62/T 2770-2017 Orchard Trenching and Fertilizing Machine—Operation Quality》, the machine's operational performance meets the design requirements.

REFERENCES

[1] Chen Y.F., (2023), *Design and experimental study of chain trenching machine in Camellia oleifera forest (油茶林链式开沟机设计与试验研究)*, MSc thesis, Central South University of Forestry and Technology, Changsha/China;

[2] Correa J., Postma J. A., Watt M., Wojciechowski T., (2019), Soil compaction and the architectural plasticity of root systems, *Journal of Experimental Botany*, vol.70, no.21, pp.6019-6034. DOI: https://doi.org/10.1093/jxb/erz383. Oxford/United Kingdom;

[3] Kang J.M., Li S.J., Yang X.J., Liu L.J., Wang C.W., (2017), Virtual simulation and power measurement of disc trencher based on multi-body dynamics (基于多体动力学的圆盘式开沟机虚拟仿真与功耗测试), *Transactions of the Chinese Society for Agricultural Machinery*, vol.48, no.1, pp.57-63. Beijing/China;

[4] Kang J. M., Li S. J., Yang X. J., Liu L J., Wang C W., Liu X Q., (2017), Design and experiment of ditching blade for ditching fertilizer applicator in densely planted orchards (密植果园开沟施肥机开沟刀片设计与试验), *Transactions of the Chinese Society for Agricultural Machinery*, vol.48, no.2, pp.68-74. Beijing/China;

[5] Liu M.Z., Xie F.P., Liu D.W., Wang X.S., (2024), Analysis and experiment of cutter roll power consumption of reverse rotary trencher based on particle scaling effect (基于颗粒放尺效应的逆旋开沟机刀辊功耗分析与试验), *Transactions of the Chinese Society of Agricultural Engineering*, vol.40, no.7, pp.83-92. Beijing/China;

[6] Liu S. X., Xu C. B., Zhang H.J., Zhang C.F., Liu X M., Wang J.X., (2019), Rack optimization design and experiment of orchard trench fertilizer applicator (果园开沟施肥机机架优化设计与试验), *Transactions of the Chinese Society for Agricultural Machinery*, vol.51, suppl.1, pp.113-122. Beijing/China;

[7] Mudarisov S., Farkhutdinov I., Khamaletdinov R., Mudarisov S., Khasanov E., Mukhametdinov A., (2022), Evaluation of the significance of the contact model particle parameters in the modelling of wet soils by the discrete element method, *Soil and Tillage Research*, vol.215, Article 105228. DOI: https://doi.org/10.1016/j.still.2021.105228 Amsterdam/The Netherlands;

[8] Ning X.Y., (2021), The significance of fertilization depth for fruit trees (果树施肥深度有讲究), *Northwest Horticulture (Fruit Trees)*, no.2, pp.42-43. Yangling/China;
[9] Peng Q. J., Kang J. M., Jian S. C., Yang X J., Liu L J., (2018), Kinematics analysis and parameter optimization of reversing ditching for disc ditching machine (圆盘开沟机反转开沟运动学分及参数优化), *Journal of China Agricultural University*, vol.23, no.8, pp.151-159. Beijing/China;
[10] Qin K., Lang X.T., Shen Z.G., Wu Z.M., Bi H.J., Cao C.M., Sun Y., Ge J., Fang L.F., (2024), Design and experiment of reciprocating furrowing and loosening machine for tea garden (茶园仿生往复式开沟松土机设计与试验), *Transactions of the Chinese Society for Agricultural Machinery*, vol.55, no.3, pp.29-39. DOI: https://doi.org/10.6041/j.issn.1000-1298.2024.03.003 Beijing/China;
[11] Qin K., Liang X.L., Cao C. M., Ding W.M., Wu Z.M., Fang L.F., (2021), Design and experiment of combined cutting and throwing ditching tool in tea garden (茶园切抛组合式开沟刀的设计与试验), *Transactions of the Chinese Society for Agricultural Machinery*, vol.52, no.5, pp.74-82. Beijing/China;
[12] Shi Z. (2019), *Research on lifting folding dual side disc type orchard ditcher (可升降折叠式双侧圆盘果园开沟机研究)*, dissertation, Huazhong Agricultural University, Wuhan/China.
[13] Song S.R., Li K., Sun D.Z., Hong T.S., Li Z., (2019), Research progress of plant protection technology and equipment in mountain orchards (山地果园植保技术与装备研究进展), *Modern Agricultural Equipment*, vol.40, no.5, pp.2-9. Nanjing/China;
[14] Wang H., Zhang W.Y., Li C.S., Wang P., Wang L.H., (2023), Research on the navigation path detection method of fruit tree drop line based on image processing (基于图像处理的果树滴水线导航路径检测方法研究), *Journal of Chinese Agricultural Mechanization*, vol.44, no.3, pp.183-190, 213. DOI: https://doi.org/10.13733/j.jcam.issn.2095-5553.2023.03.026 Beijing/China;
[15] Wang S.W., Li S.J., Zhang Y.L., Wan Q., Chen H., Meng L., (2019), Bionics of mole toe and surface heat treatment improve drag reduction and wear resistance of tooth shaped trench cutter (鼹鼠趾仿生及表面热处理提高齿形开沟刀减阻耐磨性能), *Transactions of the Chinese Society of Agricultural Engineering*, vol.35, no.12, pp.10-20. Beijing/China;
[16] Wang S.W., Li S.J., Zhang Y. L., Zhang C., Chen H., Meng L., (2018), Design and optimization of inclined spiral trenching components for mountain orchard trenching machine (山地果园开沟机倾斜螺旋式开沟部件设计与优化), *Transactions of the Chinese Society of Agricultural Engineering*, vol.34, no.23, pp.11-22. Beijing/China;
[17] Wu T., Huang W.F., Chen X.S., Ma X., Han Z.Q., Pan T., (2017), Parameter calibration of viscous soil discrete element model considering interparticle bonding force (考虑颗粒间黏结力的黏性土壤离散元模型参数标定), *Journal of South China Agricultural University*, vol.38, no.3, pp.93-98. Guangzhou/China;
[18] Yang Q., Zhang M., (2023), Effect of bio-organic fertilizers partially substituting chemical fertilizers on labile organic carbon and bacterial community of citrus orchard soils, *Plant and Soil*, vol.483, no.1-2, pp.255-272. DOI: https://doi.org/10.1007/s11104-022-05735-4 Dordrecht/The Netherlands;
[19] Zdancevičius E., Kačianauskas R., Zabulionis D., (2017), Improvement of viscoelastic damping for the Hertz contact of particles due to impact velocity, *Procedia Engineering*, vol.172, pp.1286-1290. DOI: https://doi.org/10.1016/j.proeng.2017.02.156 Amsterdam/The Netherlands;
[20] Zhang H., Xu C., Liu S., Jiang H., Liu X., Wang J., (2020), Parameter optimization and experiment of orchard double row ditching-fertilizing machine (果园双行开沟施肥机的参数优化与试验), *INMATEH Agricultural Engineering*, vol.62, no.3, pp.9-18. DOI: https://doi.org/10.35633/inmateh-62-01 Bucharest/Romania;
[21] Zhang Z.G., Wang Y., Wen B., Guo S W., Xie K T., Wang C.L., (2024), Design and travelability test of self-propelled notoginseng combined harvester (自走式三七联合收获机设计与行驶通过性试验), *Transactions of the Chinese Society for Agricultural Machinery*, vol.55, no.11, pp.306-319. Beijing/China;
[22] Zheng Y.J., Jiang S.J., Chen B.T., Lv H.D., Wan C., Kang F., (2020), Research progress on mechanization technology and equipment for orchards in hilly and mountainous areas (丘陵山区果园机械化技术与装备研究进展), *Transactions of the Chinese Society for Agricultural Machinery*, vol.51, no.11, pp.1-20. Beijing/China;
[23] Zhu X. H., Zhao H. S., Fu S.K., Li X.D., Guo W.C., Zhang L.X., (2023), Design and experiment of organic fertilizer no-trenching machine for kiwi fruit orchard (猕猴桃果园有机肥免开沟施肥机设计与试验), *Transactions of the Chinese Society for Agricultural Machinery*, vol.54, no.9, pp.133-142. Beijing/China.